



# Power-based application of frequency-averaged $\ell_1$ -norm regularisation technique for the synthesis of accelerating indoor tyre pass-by noise

Athanasios Papaioannou<sup>1,\*</sup>, Stephen J. Elliott<sup>1</sup>, Jordan Cheer<sup>1</sup>, Jacques Cuenca<sup>2</sup>, and Mansour Alkmim<sup>2,3</sup>

<sup>1</sup>Institute of Sound and Vibration Research, University of Southampton, Southampton SO17 1BJ, United Kingdom

<sup>2</sup>Siemens Digital Industries Software, 3001 Leuven, Belgium

<sup>3</sup>Department of Mechanical Engineering, KU Leuven, Celestijnenlaan 300 B, 3001 Leuven, Belgium

Received 10 May 2021, Accepted 23 October 2021

**Abstract** – Pass-by noise contribution analysis is an engineering procedure employed to estimate the contributions from various noise sources on a vehicle to the overall sound pressure level. This can be realised by placing a set of microphones close to the various sources to estimate their source strengths and then synthesising the response at a far-field linear array in the presence of the remaining sources. The results described in this paper rely on measured near-field pressure data close to the tyres of an electric vehicle under accelerating conditions. The number and position of the estimated virtual source strengths used is a compromise between complexity and accuracy, which has previously been addressed mostly empirically. A power-based, frequency-averaged  $\ell_1$ -norm regularisation technique is investigated to optimise the equivalent source position and strength for one operating tyre and, subsequently, the far-field pass-by noise pressure estimates. It is shown that for the tyre under investigation, optimising the positions of only two equivalent sources over the frequency range of interest gives a good representation of the measured far-field spectra.

**Keywords:** Inverse method, Pass-by noise, Tyre noise, Regularisation, Joint sparsity

## 1 Introduction

Vehicle pass-by noise can nowadays be measured indoors with a far-field microphone array and a stationary vehicle on a rolling road, according to ISO-362:2016 [1]. In this procedure, the various vehicle noise source contributions can also be quantified, which is described as pass-by noise contribution analysis and is nowadays widely used in automotive NVH (noise, vibration, and harshness).

The indoor pass-by noise contributions are estimated in fully operational conditions by using a set of microphones close to each component and applying the concept of acoustic transfer path analysis (TPA) [2, 3]. The sources are discretised into sets of equivalent sources, which are quantified by performing an inverse method, using the near field measured spectra and the measured transfer responses between these sources and their respective near-field microphone positions. New sets of acoustic transfer functions are then measured between the source positions and a linear microphone array 7.5 m away from the vehicle, which are then used to synthesise the far-field acoustic pressure and quantify the noise source contributions.

Tyre noise has emerged as one of the most important source contributions due to substantial efforts in reducing

engine noise and the increasing popularity of electric vehicles. While sound radiation from tyres has been rigorously studied in the past [4], various studies have been also conducted to estimate tyre noise contribution to pass-by noise in fully operational conditions. A few of these studies deploy numerical means, such as different variations of the Boundary Element Method [5, 6], to calculate vehicle pass-by noise. However, despite their good accuracy, they are mostly suited for pass-by noise estimation on the basis of the CAD/CAE computer models, early in the design stage. In [7], tyre pass-by noise is calculated experimentally using particle velocity sensors, which can prove impractical at capturing aeroacoustic phenomena, while, in [8], a separate test-bed diagnosis is needed for tyre noise estimation.

In [9], the acoustic transfer path analysis described above was used to estimate tyre noise and was proven very practical due to the small number of microphones needed close to the tyres to capture the near field spectra. This work served as the basis for a few similar studies [10–12] utilising the inverse methodology, while an alternative power-based approach was introduced in [13] and was shown to produce good results. A very similar concept was also used in [14, 15], where the need for regularisation in the inverse method was first introduced.  $\ell_2$ -norm regularisation was investigated more extensively in [16, 17], showing that it can improve tyre noise synthesis accuracy by

\*Corresponding author: [thanasispapaioan@gmail.com](mailto:thanasispapaioan@gmail.com)

avoiding source overestimation at low frequencies. Through all of this work, a predefined small set of equivalent sources is assumed to approximate tyre behaviour. The equivalent source positions are selected mainly based on the knowledge that the most dominant tyre noise phenomena occur at the tyre-road contact patch area [18, 19], the most important ones being the horn effect, which amplifies the radiation from 300 to 500 Hz upwards, and the contact forces between the tyre and the road, which create a strong vibration field close to the contact patch. The limitation stemming from using this inverse methodology is that the number and the position of the equivalent sources should be fixed and a potential investigation for the optimum source geometry would require different run-ups and significant computation time with increasing number of assumed equivalent sources, thus being very expensive.

With the aim of finding an efficient methodology to optimise the equivalent source geometry by running only one set of measurements, the work presented in [20] utilises two  $\ell_1$ -norm regularisation techniques in the inverse problem which select the equivalent source distribution, specific to the problem to be solved, from a larger set of candidate source positions based on the sparsity-promoting properties of the  $\ell_1$ -norm. The  $\ell_1$ -norm regularisation is used in a convex optimisation problem, which is calculated without inverting the transfer matrix, therefore the choice of the optimum source geometry needs significantly less computation time, even for larger number of assumed equivalent sources. The first approach is an application of  $\ell_1$ -norm regularisation at each frequency band and, thus, gives frequency-dependent source number and positioning. It has previously been investigated extensively in acoustic source identification [21–23] and near-field acoustic holography (NAH) applications with spatially confined sources [24–26], while different variations have also been proposed for more spatially distributed sources [27, 28]. Although very good results are seen using this approach, there is a different source number and positioning per frequency band, which is impractical when there is need to repeat the measurement campaign multiple times, as is often the case with pass-by noise contribution analysis. The second approach is the generalisation of  $\ell_1$ -norm regularisation for the simultaneous recovery of signals with shared sparsity properties, as documented in [29]. It provides equivalent source distributions that are fixed over frequency and thus more useful for the given problem since the optimised source geometry can then be used for subsequent measurements. This methodology is based on the principle of the simultaneous retrieval of multiple measurement vectors [30–32]. While good synthesised representations of steady-speed tyre noise with four fixed equivalent source distributions were seen with this method in [20], using the linear, phase-dependent problem formulation incurred significant phase-related errors in the tyre noise far-field synthesis, in line with what was previously described in [33, 34].

Since the calculation of the SPL for pass-by noise engineering purposes does not require the use of the phase information and in an effort to alleviate the effect of the phase-related errors, this paper focuses on the investigation

of the frequency-averaged  $\ell_1$ -norm regularisation, which was formulated in [20], using a power-based formulation, similar to the one presented in [13]. The new power-based, frequency-averaged  $\ell_1$ -norm regularisation as a means of optimising the equivalent source distribution, which is the novelty of this work, omits the phase information, while the equivalent source strength cross spectra are also not taken into account, in an effort to keep the complexity of the regularisation problem to a minimum. A full vehicle indoor pass-by noise test campaign is also performed using accelerating tyre noise data and with the vehicle operated under fully operational conditions, in order to assess the performance of the methodology. The accelerating near-field tyre noise data and the corresponding measured transfer responses are used in the convex optimisation problem to estimate the optimum source geometry and reconstruct the equivalent source distribution. The distribution is then used, together with measured far-field transfer responses, for far-field tyre noise synthesis. The aim of this paper is therefore to investigate the application of the power-based, frequency-averaged  $\ell_1$ -norm regularisation method to optimise the equivalent source geometry and far-field synthesised spectra for various numbers of sources without assuming prior knowledge of the noise – generating mechanisms of the tyre.

In Section 2, the power-based methodology used for the tyre noise synthesis including the frequency-averaged  $\ell_1$ -norm regularisation is covered, while, in Section 3, the measurement set-ups are presented. The corresponding results are discussed in Section 4, while the conclusions drawn are covered in Section 5.

## 2 Formulation

### 2.1 Power-based, frequency-averaged $\ell_1$ -norm regularisation

As a first step, the pressure is assumed to be measured with a near-field array of  $M$  microphones. The accelerating tyre noise has a time dependence that can be regarded as random with non-stationary statistical properties. For the purposes of the frequency-domain formulation used in this paper, the power spectral densities are estimated by averaging the modulus squared spectra over multiple overlapping short segments of data in the time-domain, where the pressure signals are locally assumed stationary [35]. Assuming  $x$  time segments, for each segment of period  $T_r$ , the raw periodogram is formed as

$$\hat{S}_{p_{near,i}}(f) = \frac{1}{T_r} |X_{T_{r,i}}(f)|^2 \quad \text{for } i = 1, 2, \dots, x, \quad (1)$$

where  $X_{T_{r,i}}(f)$  denotes the Fourier transform at a certain frequency  $f$ . The power spectral density at the  $m$ -th microphone for the given frequency is then defined by

$$S_{p_{near,m}}(f) = \frac{1}{x} \sum_{i=1}^x \hat{S}_{p_{near,m}}(f). \quad (2)$$

These spectra will in practice be contaminated by errors and noise. The tyre radiation is approximated by  $L$

monopoles distributed over its radiating surface with source strength power spectral densities  $\mathbf{S}_q$ , while the transfer paths between the equivalent sources and the near-field microphones are estimated by means of the squared modulus of a frequency response function matrix  $|\mathbf{G}_{\text{near}}|^2$  of size  $M \times L$  which in practice should also be measured. Therefore, the equation describing the system at a given frequency is

$$\mathbf{S}_{\text{pnear}} = |\mathbf{G}_{\text{near}}|^2 \mathbf{S}_q + \mathbf{S}_e, \quad (3)$$

where  $\mathbf{S}_{\text{pnear}}$  is a vector of  $S_{\text{pnear}}(f)$  at the  $M$  near-field microphones and  $\mathbf{S}_e$  is a vector of real errors.

Similarly to the method described in [20], the total number of possible equivalent source positions can be greater than the number of near-field microphones (i.e.  $L > M$ ). Sparsity in  $\mathbf{S}_q$  is introduced by solving the linear problem, while constraining the  $\ell_1$ -norm of the source strength vectors over frequency. A new matrix  $\mathbf{S}_Q$  is formed, whose columns are the source strength vectors  $\mathbf{S}_q(\omega_k)$  at each frequency line  $k$  of total number  $K$ . The frequency-averaged  $\ell_1$ -norm of this matrix of size  $L \times K$  is expressed mathematically by the  $\ell_{1,2}$ -norm. The  $l$ -th row of  $\mathbf{S}_Q$  is  $\mathbf{S}_q^l = [S_q^l[K_1], \dots, S_q^l[K_2]]$  and the frequency-averaged norm of  $\mathbf{S}_Q$  is then defined as

$$\|\mathbf{S}_Q\|_{1,2} = \sum_{l=1}^L \left( \left\| \mathbf{S}_q^l \right\|_2 \right)^1 = \sum_{l=1}^L \left( \sum_{k=K_1}^{K_2} |S_q^l[k]|^2 \right)^{1/2}, \quad (4)$$

where  $K_1$  and  $K_2$  define the frequency range for which the problem is solved. By constraining this norm to a low maximum value which is dependent on the magnitude of the source strength vector over frequency and, in this paper, is found by trial-and-error, the vectors  $\mathbf{S}_q$  are jointly decomposed as a combination of a number of elements equal to  $L_f$ , which is a subset of the number of source positions  $L$  (i.e.  $L \geq L_f$ ). When the number of non-zero point sources gets smaller or equal to the number of near-field microphones ( $L > M \geq L_f$ ), the final system of equations becomes resolvable in the constrained minimisation problem

$$\min_{\mathbf{S}_Q} \sum_{k=K_1}^{K_2} \left\| |\mathbf{G}_{\text{near}}|^2(\omega_k) \mathbf{S}_q(\omega_k) - \mathbf{S}_{\text{pnear}}(\omega_k) \right\|_2 \quad (5)$$

subject to  $\|\mathbf{S}_Q\|_{1,2} \leq \alpha$ .

Parameter  $\alpha$  is a scalar, which modulates the maximum value of  $\|\mathbf{S}_Q\|_{1,2}$  and, thus, sets the ceiling for the sum of the power spectral densities of the source strength vectors over frequency. By assigning a low value to  $\alpha$ , the problem is constrained to be solved with a number of sources smaller than the original set, thus introducing sparsity. A common sparsity profile for the various frequency lines is introduced, which translates to a number of non-zero equivalent source positions in the source vector, which are fixed over frequency [36]. The lower the value of  $\alpha$ , the more it will enforce sparsity in the solution and thus a smaller number of non-zero equivalent sources will be used in the linear problem. This constrained optimisation can, therefore,

estimate source strength power vectors  $\mathbf{S}_q$  which share the same sparsity pattern with respect to the source positions and minimise the sum of the least-squares linear problem over frequency. The SPGL1 toolbox is used to solve the problem [37–38].

After the use of the frequency-averaged  $\ell_1$ -norm regularisation technique, the problem is reduced to a determined or overdetermined one with a reduced vector of source power spectra  $\mathbf{S}'_q$  of size  $L_f \times 1$  and a reduced modulus-squared transfer response function matrix  $|\mathbf{G}'_{\text{near}}|^2$  with size  $M \times L_f$ , where  $M \geq L_f$ . The inverse problem is then solved using the squared modulus pseudo-inverse  $|\mathbf{G}'_{\text{near}}|^2{}^+$  formed between the non-zero source components and the near-field microphones

$$\mathbf{S}'_q = |\mathbf{G}'_{\text{near}}|^2{}^+ \mathbf{S}_{\text{pnear}}. \quad (6)$$

## 2.2 Far-field pressure synthesis

The power spectral density of the sound pressure in the linear far-field array is estimated by

$$\tilde{\mathbf{S}}_{\text{pfar}} = |\mathbf{G}'_{\text{far}}|^2 \mathbf{S}'_q, \quad (7)$$

where  $|\mathbf{G}'_{\text{far}}|^2$  is the modulus-squared transfer response matrix connecting the far-field microphones to the non-zero equivalent source positions, and, in practice, should also be measured. The sound pressure level of the estimated  $\text{SPL}_t$  is energetically added to those corresponding to the remaining sources on the vehicle which are not under investigation, and are quantified by assuming a fixed small number of sources close to each source and performing the same power-based inverse methodology. Assuming  $Z$  remaining sources, the final synthesised far-field response  $\tilde{\text{SPL}}_{\text{ov}}$  at each microphone is the sum of the tyre noise contribution and the remaining synthesised noise source contributions

$$\tilde{\text{SPL}}_{\text{ov}} = 10 \log_{10} \left( 10^{\frac{\text{SPL}_t}{10}} + 10^{\frac{\text{SPL}_1}{10}} + \dots + 10^{\frac{\text{SPL}_Z}{10}} \right), \quad (8)$$

which is compared to  $\tilde{\text{SPL}}_{\text{ov}}$ , the response measured directly using a far-field microphone array.

Since the equivalent source investigation is done only for the noise emitted from one accelerating tyre, the synthesised contributions of the remaining sources are fixed pressure level curves and their accuracy should be validated upfront to guarantee reliable source investigation results. These sources could be the remaining tyres, the engine, the gearbox, etc. It is important to state that adding the noise source contributions energetically, which assumes that all of the sources are entirely uncorrelated, could be a limiting factor for this approach. A diagram illustrating the signals and optimisation processes involved in this section is given in Figure 1.

To sum up, the work presented in this paper aims to tackle the susceptibility of the synthesis problem to phase-related errors by eliminating the phase information

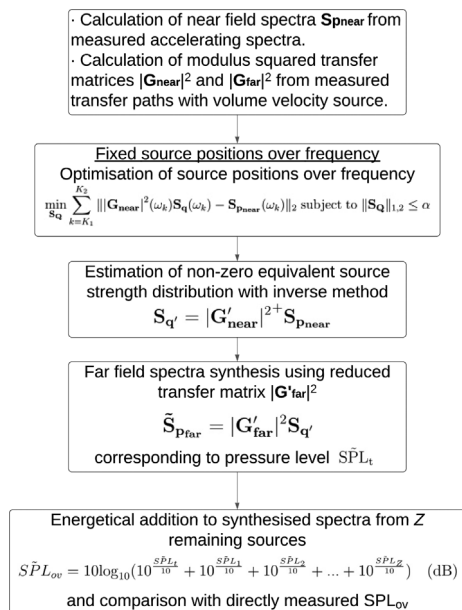


**Figure 1.** Diagram illustrating the signal acquisition and optimisation process described in Section 2.

in the transfer matrix and estimating only the power spectral densities of the source strengths, thus assuming that the sources are uncorrelated. The source geometry selection for a given number of sources and over the frequency range of interest is performed by using the frequency-averaged  $\ell_1$ -norm regularisation technique, which was investigated in [20], in order to directly associate the choice of the equivalent source positions with the cost function to be minimised. In this approach, the regularisation is used to identify the positioning of the minimum number of equivalent sources needed for a given synthesis accuracy and then the power-based inverse problem is performed, using a pseudo-inverse that corresponds to the selected source geometry. The final source strength amplitudes are then used to synthesise the far-field pressure, which is added energetically to the synthesised responses from the remaining sources on the car. The overall response is finally compared to the one measured directly by the far-field linear array.

### 3 Experimental validation

The method described in Section 2 was validated on a full vehicle indoor pass-by noise measurement campaign. The vehicle used was a SimRod rear-wheel drive electric car developed for Siemens by Kyburz, Switzerland, as a test version of the commercial eRod vehicle. Tyres of type Pirelli 195/50R15 with radius 28.8 cm were used. The experiment was split into two measurement sessions which took place in the semi anechoic chamber at Siemens Digital Industries Software.<sup>1</sup>

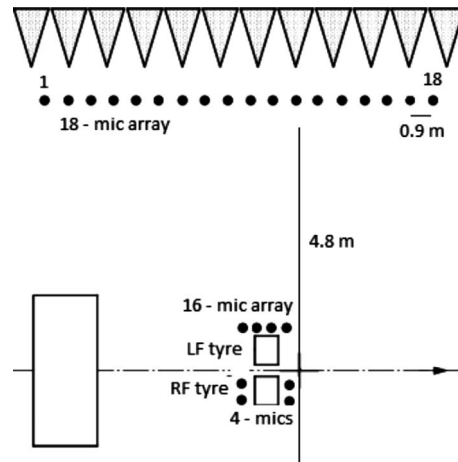


**Figure 2.** Schematic of the 1st measurement set up.

#### 3.1 Front tyre noise measurements with engine off

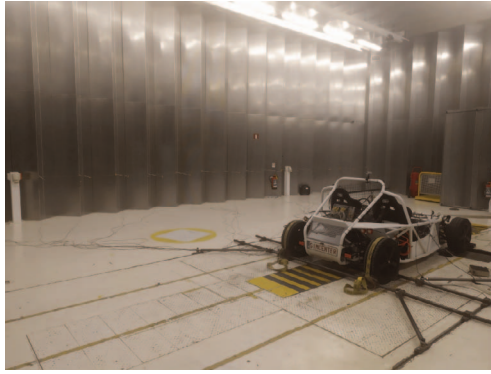
In the first instance, the left front (LF) tyre was selected as the tyre under investigation when only noise from the two front tyres was emitted. The vehicle was fixed so that its front tyres were placed on top of the rolling road with a smooth road surface, which was controlled by one motor for both tyres. A schematic of the measurement set up is given in Figure 2.

Eighteen microphones were placed in a linear array 4.8 m away from the left side of the car, as shown in Figure 3a. The microphone height was set to 1 m, while the microphone spacing was set to 0.9 m with a 15.3 m total array length. A near-field circular array of 16 microphones with a radius of 29 cm was placed 15 cm away from the left front tyre, as shown in Figure 3b. The microphone number was chosen to be double the number of the maximum equivalent sources assumed within the investigation. 4 microphones were placed close to the right front (RF) tyre, 2 on the leading edge and 2 on the trailing edge of the tyre.

The car was not in operation and, instead, the rolling road was driven to excite the front tyres, therefore the two front tyres were the only noise-emitting sources. The pressure was measured at an acceleration of  $1 \text{ m/s}^2$ , from 5 to 60 km/h. The time signal measured at a microphone in the near-field circular array, as well as its corresponding spectrogram, is given in Figure 4. The increasing speed is highlighted by the increase in the pressure amplitude, while, in the spectrogram, it is shown that the increase in the rolling speed is associated with increasing frequency.

The next step was the measurement of the transfer responses between the microphone arrays and the candidate equivalent source positions distributed close to the tyres, which were herein represented by the measured Frequency Response Functions (FRFs). For this purpose, an omni-directional Simcenter Qsources Mid-High-frequency (Q-MHF) volume velocity source, covering the range between 100 and 10,000 Hz, was used [39]. The source was moved to the various candidate source positions in order to measure the individual FRFs. For the left front tyre under investigation, 12 equivalent source positions were assumed,

<sup>1</sup> <https://www.sw.siemens.com/>.



(a)



(b)

**Figure 3.** (a) Fixed Simrod with front tyres on rolling road and far-field microphone array in the Siemens semi-anechoic chamber, (b) near-field microphone array close to the left front tyre.

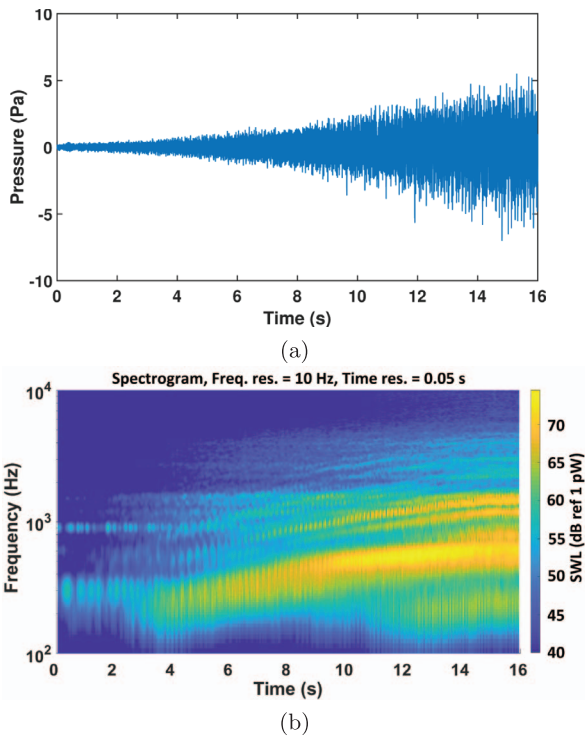
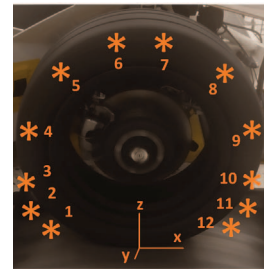


**Figure 4.** (a) Pressure signal measured at the near-field circular microphone array for  $1 \text{ m/s}^2$  acceleration; (b) Spectrogram of the near-field pressure signals for  $1 \text{ m/s}^2$  acceleration.

**Table 1.** Coordinates of the candidate equivalent sources for the tyre under investigation.

Source No.	X (cm)	Y (cm)	Z (cm)
1	-20.5	-5	-24
2	-23.5	-1	-17
3	-25.5	-0.5	-8
4	-25	0.5	5
5	-18	0.5	20
6	-4	0.5	26
7	5	0.5	26
8	18	0.5	18
9	25	0.5	5
10	25.5	-0.5	-8
11	23.5	-1	-17
12	20.5	-5	-23



(a)



(b)

**Figure 5.** (a) Equivalent source position grid for left front tyre under investigation; (b) Equivalent source positions for right front tyre.

distributed along the tyre circumference starting from the leading edge towards the trailing edge, as shown in [Figure 5a](#). The distance between the candidate equivalent sources close to the contact patch is approximately 5 cm, while, moving away from the patches, the distance is 12–15 cm. For the right front tyre, two equivalent sources were assumed in the middle of the contact patch, one at each edge of the tyre, as shown in [Figure 5b](#). Assuming that the centre of the tyre is a point with coordinates  $(0, 0, 0)$ , [Table 1](#) gives the detailed coordinates of the 12 candidate equivalent sources in cm for the tyre under investigation.

The FRFs were measured between the 12 source positions and both the far-field linear array and the near-field circular array, while, for the other tyre, the transfer responses were then measured between the two source positions and both the far-field linear array and the four microphones placed close to the tyre. Each FRF was calculated by dividing the response at each microphone by the source strength obtained by the volume velocity source at each source position. Fully coupled matrices representing the transfer paths between the microphone arrays and the source positions were therefore calculated at each frequency line over the range of 100–10,000 Hz with a frequency resolution of 5 Hz. An example of the amplitude of the transfer response between far-field microphone No. 10 and the

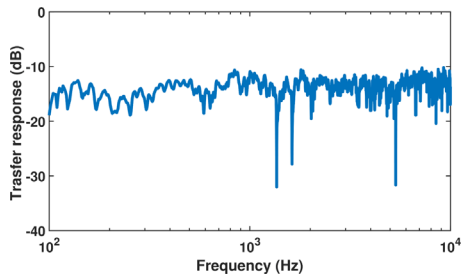


**Figure 6.** Amplitude of the transfer response between far-field mic No. 10 and equivalent source on the leading edge of the left front tyre.

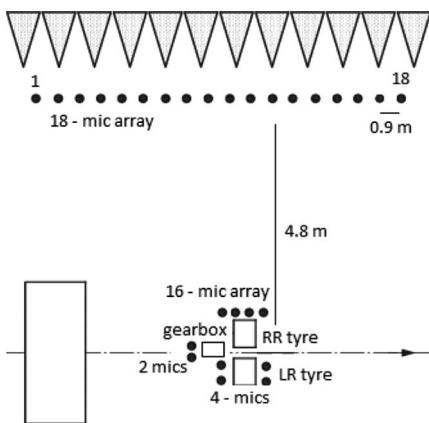


**Figure 7.** Schematic of the 2nd measurement set up.

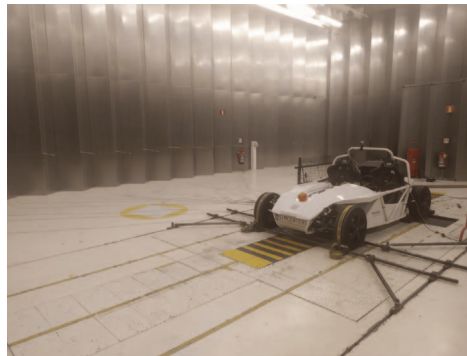
source position on the leading edge of the left front tyre is given in Figure 6 for reference.

**3.2 Rear tyre noise measurements in fully operational conditions**

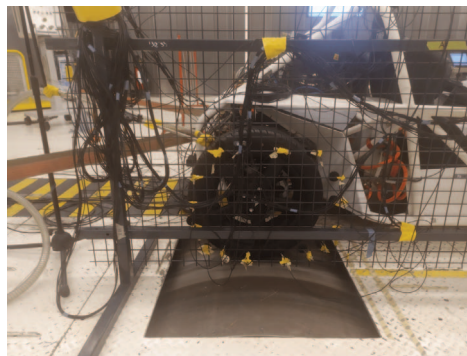
The purpose of the second measurement session was to test the accuracy of the frequency averaged  $\ell_1$ -norm regularisation in predicting the number and positions of the equivalent sources for synthesising the far-field response of one tyre with the vehicle in fully operational conditions. The tyre under source investigation was the right rear tyre, while the sources acting simultaneously were the two rear tyres and the gearbox. A schematic of the measurement set up is given in Figure 7.

In this session, the vehicle was fixed in the designated area so that its rear tyres were placed on top of the rolling road. The same linear far-field array was used 4.8 m away from the car, as shown in Figure 8a, and the same near-field circular array was placed 15 cm away from the right rear tyre, as shown in Figure 8b. Finally, four microphones were placed close to the left rear tyre, two on the leading edge and two on the trailing edge of the tyre, and two microphones were placed close to the gearbox.

In these measurements, the car was driven while the rolling road was operated in a minimal resistance mode, which means that no manual exterior force was exercised at the rolling road to counter against the movement of

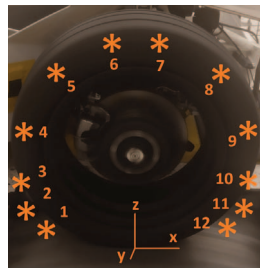


(a)



(b)

**Figure 8.** (a) Fixed SimRod vehicle with rear tyres on rolling road and far-field microphone array in the Siemens semi-anechoic chamber; (b) Near-field microphone array close to the right rear tyre.



(a)



(b)



(c)

**Figure 9.** (a) Equivalent source position grid for right rear tyre under investigation; (b) Equivalent source positions for left rear tyre; (c) Equivalent source position for gearbox.

the tyres. The pressure spectrum was measured at all the various microphones from 5 to 60 km/h with an acceleration of  $1 \text{ m/s}^2$ . The volume velocity source was then used to measure the transfer responses between the 12 equivalent source positions along the right rear tyre circumference and both the far-field linear and the near-field circular array. The same positioning as in Section 3.1 was used for the equivalent sources of the tyre under investigation. Corresponding FRFs were also measured for the two equivalent sources, one at the centre of the contact patch of each edge of the left rear tyre, and for the one equivalent source close to the gearbox. Fully coupled matrices were, therefore, calculated between the equivalent source positions and their corresponding far-field and near-field microphones at each frequency line over the frequency range of interest (100–10,000 Hz). An overview of the equivalent source positions assumed in this measurement set up is given in Figure 9.

## 4 Results from measurements of front tyre noise with engine off

### 4.1 Choice of source positions with $\ell_1$ -norm regularisation technique

The first step of the analysis was the use of the power-based, frequency-averaged  $\ell_1$ -norm regularisation to optimise the source distribution for various numbers of equivalent sources from the grid of the 12 source positions. To accomplish that, the optimisation problem was solved for a range of values of the regularisation parameter  $\alpha$ , which resulted in the use of a small number of non-zero sources out of the 12, specifically 1–8 sources for different values of  $\alpha$ . Each value of  $\alpha$  gives a different solution to the optimisation problem and is, therefore, associated with a specific non-zero source number and geometry.

In Figure 10a, the relationship between the regularisation parameter  $\alpha$  and the number of non-zero sources used in the frequency-averaged inverse problem is given, while, in Figure 10b, the sum of the least-squares residuals over frequency is shown with respect to  $\alpha$ . It is shown that a given range of  $\alpha$  corresponds to the use of a given number of non-zero sources out of the 12. It is also seen from these results that there is a set of regularisation parameters, primarily translating to the use of two equivalent sources, where the error decreases substantially whereas the use of a higher number of sources is not shown to further improve the reconstruction accuracy. Therefore, using two equivalent sources seems to be the optimum strategy, which is an improvement compared to the four-source optimum strategy seen in [20]. The best geometry for each number of non-zero sources is selected by choosing the value of  $\alpha$  which gives the minimum least-squares error over frequency. For example, sweeping  $\alpha$  from 0.002 to 0.02 gives different solutions of 2 non-zero sources out of the 12. The one which is chosen is the one which gives the minimum error over frequency for this range of  $\alpha$ , as shown in Figure 10b.

In Figure 11, the equivalent source positions are given using the frequency-averaged  $\ell_1$ -norm regularisation for 1, 2, 4 and 8 equivalent sources. For a small number of

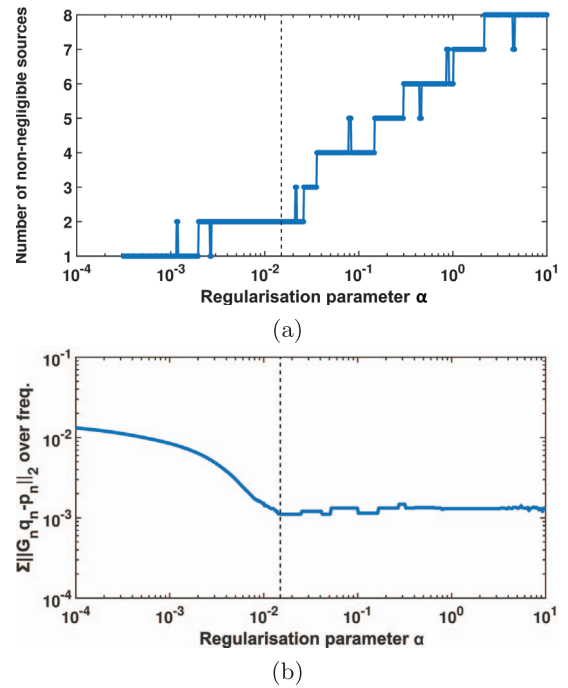


**Figure 10.** Relationship between regularisation parameter  $\alpha$  with (a) number of non-zero sources and (b) near-field problem least-squares residual.

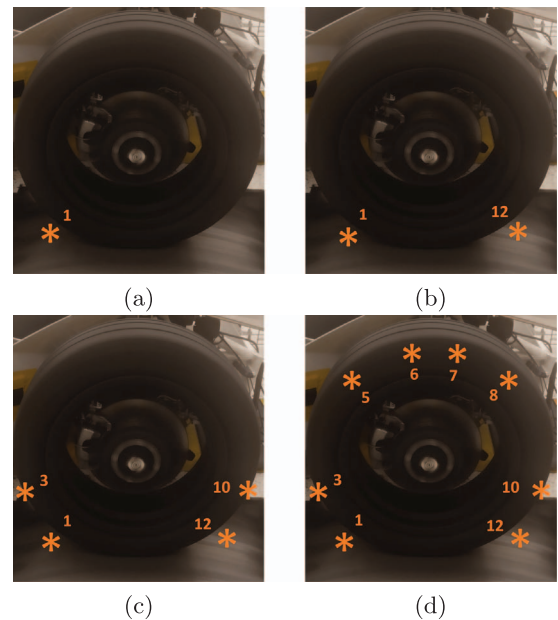


**Figure 11.** Equivalent source positions using the frequency averaged  $\ell_1$ -norm regularisation for (a) 1, (b) 2, (c) 4 and (d) 8 equivalent sources.

sources, the source positions are concentrated towards the leading and trailing edge of the tyre, where the tyre noise phenomena are known to be dominant, while using a higher number of sources spreads their distribution around the circumference of the tyre. It is, however, important to add that the exact positioning of the sources might not be the optimum one from a physical standpoint. More testing

using a finer source grid would have to be performed to address this.

An exhaustive search of the equivalent source positioning was also conducted using 1, 2, 4 and 8 equivalent sources out of the 12 and the distributions were seen to be very close to the ones obtained using the  $\ell_1$  regularisation method. The computational complexity of the exhaustive research was substantially larger, with the simulations starting from a few minutes for the 1-source case and going up to an hour when the eight equivalent sources were used, while the computation time using the  $\ell_1$ -norm regularisation techniques was within 30 s for the various numbers of equivalent sources for a 4-core, 1 GHz, computer.

## 4.2 Far-field pressure synthesis

The next step in the analysis was the utilisation of the equivalent source strengths to synthesise the far-field response of the left and right tyre and add them energetically. The final synthesised response was then compared to the one measured directly.

In Figure 12, the synthesised SPL in 1/3 octave bands at far-field microphone No. 11 is given over the frequency range of interest for the left front tyre using the regularisation technique with various numbers of equivalent sources and for the right front tyre using two predefined sources. The two responses were energetically added and the final synthesised response was compared to the one measured directly at the far-field linear array. The results for microphone No. 11 were chosen as it is the one which is subject to the highest acoustic response for the  $1 \text{ m/s}^2$  case. The directly measured spectra reveal a dominant region between 400 Hz and 1.5 kHz, although a small dip is identified around 800 Hz. The synthesised response for the right front tyre is the same for all the various cases as it is not dependent on the  $\ell_1$ -norm regularisation investigation.

For the one-source case, the accuracy is very acceptable up to approximately 1.5 kHz, while using two sources extends the accuracy up to approximately 3 kHz. This is a substantial improvement compared to the accuracy achieved taking the coherence and phase information into account in [20] and is due to the ability of the power-based method to create larger patches on the tyre with an average source strength. For a higher number of sources, the reconstruction accuracy improves even at higher frequencies. However, this improvement is not critical since the response from the tyre above 3 kHz is attenuated significantly compared to the dominant response between 400 Hz and 1.5 kHz. This is in line with the results in Figure 10, where it was seen that no significant improvement should be expected when using more than two equivalent sources. The overestimation of the response at low frequencies, which was seen in [20], is limited since the phase information, which is the most important reason for the creation of errors during the transfer matrix inversion, is not taken into account. However, it is seen that the overestimation worsens by increasing number of equivalent sources, which could be due to the fact that, at low frequencies, the tyre geometry dimensions are small in comparison to the

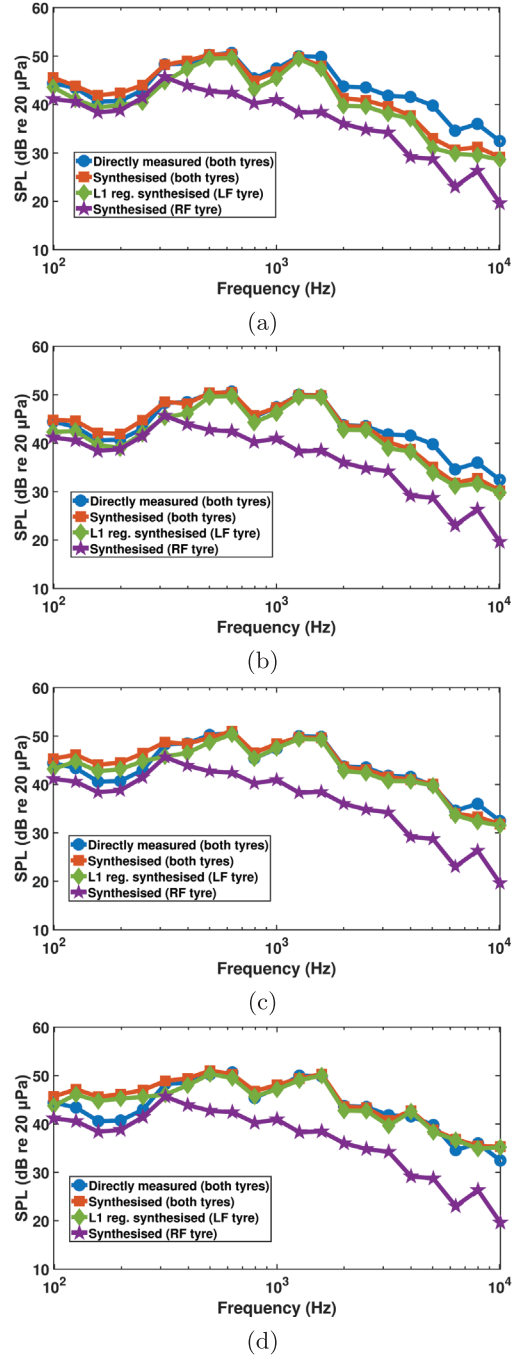


**Figure 12.** SPL in 1/3 octave bands at far-field microphone 11 over the frequency range with the left front tyre synthesis performed using (a) 1 equivalent source, (b) 2 equivalent sources, (c) 4 equivalent sources and (d) 8 equivalent sources.

wavelength in air and, thus, a one source solution gives the best results.

## 4.3 Results across far-field array

The far-field pressure synthesis accuracy with the considered method was further investigated across the far-field microphone array by taking into account the overall pressure response over the frequency range of interest.

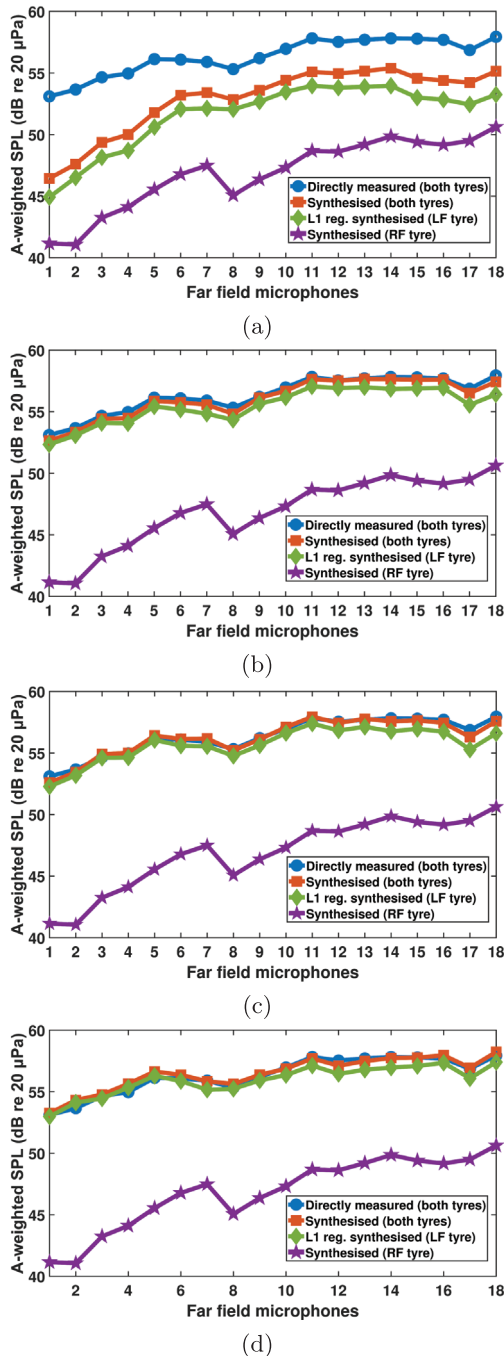


**Figure 13.** A-weighted SPL across the far-field array using (a) 1, (b) 2, (c) 4 and (d) 8 fixed sources for the left front tyre over frequency compared to the directly measured spectra.

In [Figure 13](#), the A-weighted SPL across the far-field microphone array is shown for the synthesised contribution of the left front tyre with various numbers of equivalent sources, the synthesised contribution of the right front tyre and their summed synthesised response which is compared to the directly measured response. Using one source to discretise the left front tyre gives an average deviation of 3.5 dB over the microphone array, while adding one more

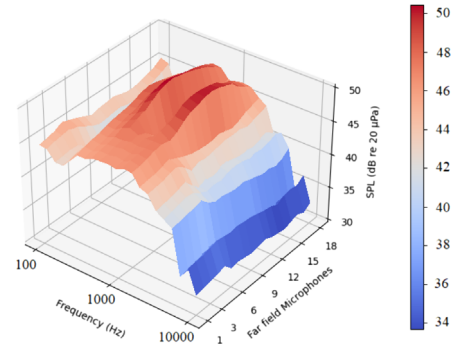


**Figure 14.** SPL at the various frequency bins and across the far field microphone array for the case of 2 fixed equivalent sources.

source reduces this deviation to only 0.4 dB. Using 4 and 8 sources give deviations of approximately 0.3 and 0.4 dB respectively. Therefore, considering the need for the minimisation of the number of equivalent sources used identifies the use of two sources, one on the leading edge and one on the trailing edge of the left front tyre, as the optimum strategy with the given inverse problem formulation. It is, however, important to highlight that the accuracy of the far-field synthesised response also depends upon the accuracy of the right front tyre synthesised response, which was computed following the inverse methodology with two fixed equivalent sources.

Finally, in [Figure 14](#), a surface plot of the SPL at the various frequency bins and across the far field microphone array is given for the case of two fixed equivalent sources. It is shown that, while for microphones 9–15, which are closer to the tyres, the response between 400 Hz and 1.5 kHz is dominant, a change in the frequency response is seen moving away from the tyres. The response at the 400 Hz – 1.5 kHz decreases and flattens, possibly indicating a decrease in the impact of the horn effect for these microphones, which is known to be dominant at this frequency range. An increase in the response is also seen at low frequencies for microphones 1–3 and 17–18. This could indicate an increase in the effect of the vibration field of the tyre at those angles, which is more dominant at low frequencies, assuming that there is no impact from placing the microphones close to the walls.

## 5 Results from measurements of rear tyre noise in fully operational conditions

In this section, a more challenging synthesis concept was tested using data from fully operational measurement conditions, as presented in [Section 3.2](#).

In [Figure 15](#), a comparison between the measured spectra at far field microphone No. 11 is shown for the two measurement set-ups described in [Sections 3.1](#) and [3.2](#). The spectra measured in the fully operational case are higher throughout the frequency range of interest, with the exception of a region around 300–400 Hz and at 1.7 kHz where

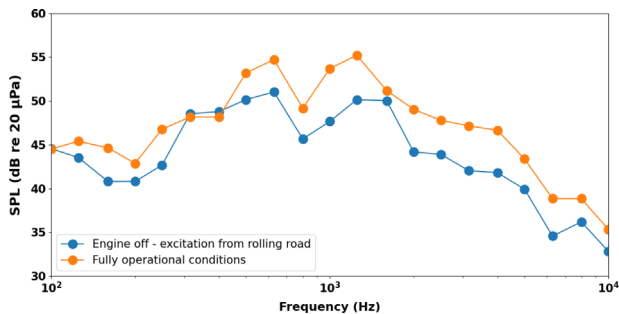


**Figure 15.** SPL in 1/3 octave bands at far-field microphone 11 over the frequency range for the measurements described in Sections 3.1 and 3.2.

the responses are very similar, although a smaller increase at low frequencies is seen. A similar pattern is seen in terms of the dominant frequencies of the spectra, as the range between 500 Hz and 1.5 kHz is the strongest with the exception of a dip at 800 Hz for both set-ups.

The power-based, frequency-averaged  $\ell_1$ -norm regularisation was used to decide the number and position of the equivalent sources for the right rear tyre under the presence of noise emitted also by the left rear tyre and the gearbox. Different synthesised curves for the right rear tyre were obtained for different numbers of equivalent sources and these were added energetically to the synthesised curves using two fixed sources for the left rear tyre and one fixed source for the gearbox. The overall synthesised spectra were then compared to the one measured directly. The analysis was again done for a car driven from 5 to 60 km/h with a  $1 \text{ m/s}^2$  acceleration using 1, 2, 4 and 8 equivalent sources for the right rear tyre. It is important to add that the source number and positioning for the remaining sources were chosen by experience and could be a possible source of error in the estimation.

By performing the  $\ell_1$ -norm regularisation in the power-based formulation it was shown that the set of regularisation parameters where the error decreases substantially translates to the use of two sources whereas the use of a higher number of sources was not shown to further improve the reconstruction accuracy. Once again, in order to choose the equivalent source positions, the regularisation parameter that minimises the least-squares error over frequency was chosen within the range of the parameter which results in the use of a chosen number of non-zero sources. This is done for the cases of 1, 2, 4 and 8 equivalent sources.

The fixed positions chosen using the  $\ell_1$ -norm regularisation are given in Figure 16. From these results it can be seen that the same pattern as in the previous sections is followed starting from only one source position on the leading edge of the tyre to two on both edges and then an expansion around the circumference of the tyre. However, in this case, the sources are not symmetrical, which could be due to a number of reasons, some of which are potential added noise accumulated at the near-field microphones from the operating vehicle or non-symmetrical radiation from the tyre under fully operational conditions. Further research would be needed to address this.

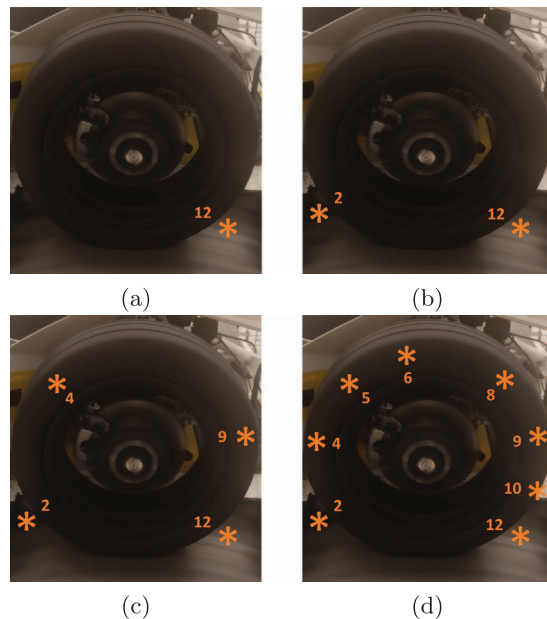


**Figure 16.** Equivalent source positions using the frequency averaged  $\ell_1$  regularisation for (a) 1, (b) 2, (c) 4 and (d) 8 equivalent sources.

After selecting the equivalent source positions, the inverse and forward method were performed for each noise source component independently and the corresponding synthesised contributions were obtained for the far-field linear array. The gearbox contribution was synthesised using one equivalent source, the left rear tyre contribution using two equivalent sources, while the right rear tyre contribution, which was the one under investigation, was approximated using the geometries retrieved with the  $\ell_1$ -norm regularisation. The various contributions were then added energetically and the final synthesised response was compared to the one measured directly.

In Figure 17, the synthesised SPL in 1/3 octave bands at far-field microphone No. 11 is given over the frequency range of interest for the right rear tyre using the regularisation technique with various numbers of equivalent sources, the fixed response from the remaining sources, as well as their overall synthesised response. The results for microphone No. 11 are chosen as it is again the one that is subject to the highest acoustic response for the  $1 \text{ m/s}^2$  case. The synthesised responses for the left rear tyre and the gearbox are the same for all the various cases since they are not dependent on the  $\ell_1$ -norm regularisation investigation. In the left rear tyre response, two dominant frequencies are seen, the first one around 600 Hz and the second one at 1 kHz. In the gearbox response, three dominant regions are distinguished at 650 Hz, 1.4 kHz and 3 kHz and could be either due to the engine harmonics, which can be proven with an experimental vibration investigation on the motor/transmission, or due to tyre noise leakage into the gearbox microphone signal despite the low level of the gearbox contribution.

Using one equivalent source for the right rear tyre synthesised response gives an overall acceptable accuracy up to

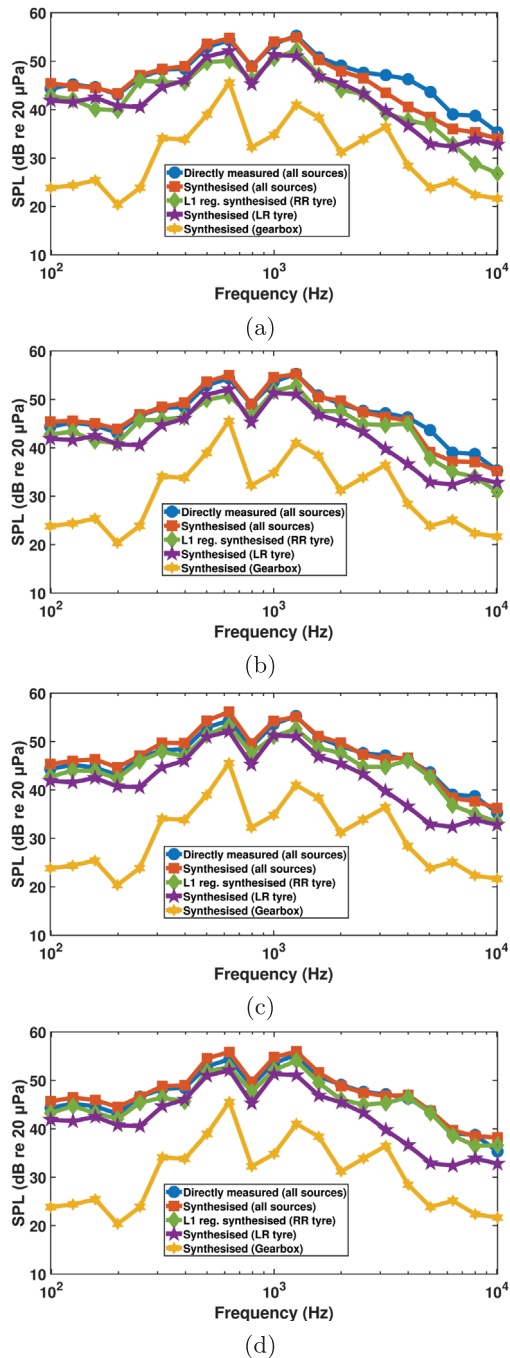


**Figure 17.** SPL in 1/3 octave bands at far-field microphone 11 over the frequency range with the right rear tyre synthesis performed using (a) 1 equivalent source, (b) 2 equivalent sources, (c) 4 equivalent sources and (d) 8 equivalent sources.

approximately 2 kHz, while using two sources extends the accuracy up to approximately 4 kHz. These frequency limits up to which the reconstruction is good are substantially higher than the ones seen in the tyre-noise-only case. For larger number of sources, a slight overestimation of the directly measured response is seen up to approximately 1.5 kHz, while at higher frequencies the synthesised

response is a better representation of the direct response. Compared to the results from the first measurement set-up, a better synthesis accuracy is seen at low frequencies using 2 or 4 sources. The fact that using one source gives a better representation of the final response up to higher frequencies than expected and that the response is overestimated for eight sources should probably be attributed to an overestimation of one or more of the individual source contributions.

The trend highlighted above is also depicted in the A-weighted SPL across the microphone array, which is presented in Figure 18. Using one source to discretise the right rear tyre gives an average deviation of 2 dB over the microphone array, while adding 1 more source reduces this deviation to only 0.5 dB. Using 4 and 8 sources gives deviations of approximately 0.6 and 0.9 dB respectively. The small deviation seen in the one-source case, as well as the overestimation of the response in the eight-source case, is not in agreement with the results of the  $\ell_1$ -norm regularisation and could imply an overestimation of one or more of the individual contributions. This could be either due to errors in the power-based inverse method or due to the added noise captured by the near-field microphones in fully operational conditions. Assessing the near-field microphone contamination as the possible cause for the overestimation would require additional signal processing methodologies.

In Figure 19, the SPL surface plot at the various frequency bins and across the far field microphone array is again given for the case of two fixed equivalent sources. While the response at the frequency range between 400 Hz and 1.5 kHz is dominant at microphones 8–15, it gradually decreases towards the edges of the far field array, albeit not at the same rate compared to the one seen in Figure 14. The response at low frequencies and between 1.5 kHz and 3 kHz is also seen to increase at microphones 1–4 and 16–18.

Further research would be needed to assess the effect of the candidate source grid and the source type to the source selection. While the candidate source grid was limited to 12 monopole sources in this case to accommodate the measurement campaign, a finer grid of sources or the choice of alternative source types (dipoles, quadrupoles, etc.) could potentially lead to different source selection and synthesis results. Further research would also be needed to assess the performance of the method when the radiation conditions vary substantially as the frequency-averaged source selection, which is performed in this methodology, could potentially lead to poor reconstruction accuracy.

Nevertheless, in this case, considering the need for the minimisation of the number of used equivalent sources, the use of two sources on the leading and trailing edges of the right rear tyre was identified as the optimum strategy with the given inverse problem formulation. Assuming that the synthesis estimate provided from the left rear tyre and the gearbox are reasonably accurate, this is an improved result compared to the investigation done in [20]. Although not presented herein, the same analysis was also performed

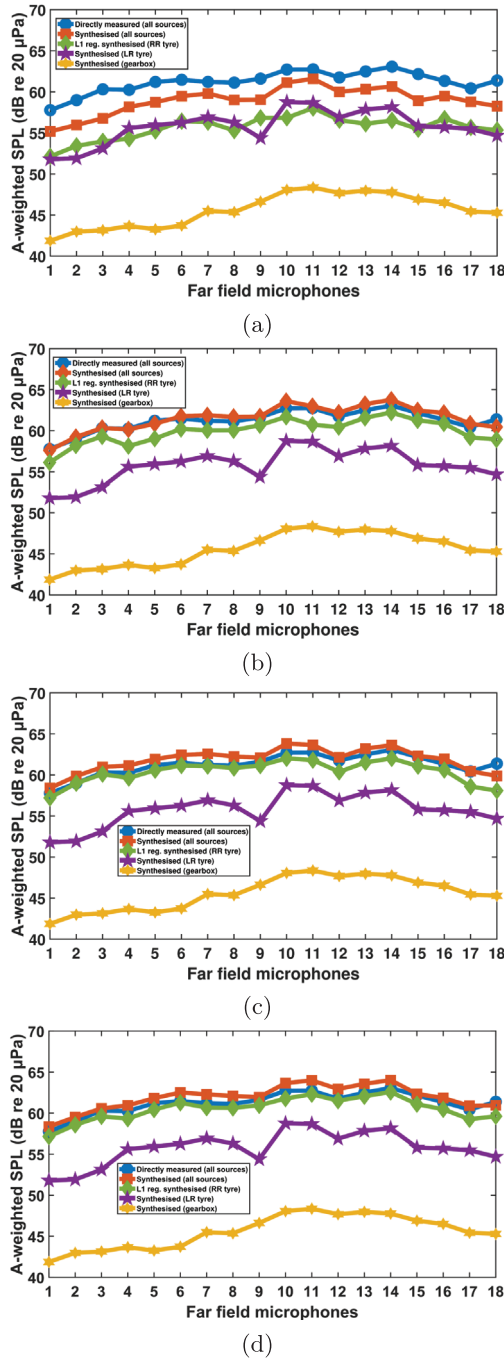


**Figure 18.** A-weighted SPL across the far-field array using (a) 1, (b) 2, (c) 4 and (d) 8 fixed sources for the right rear tyre reconstruction over frequency compared to the directly measured spectra.

for the  $2 \text{ m/s}^2$  acceleration case and very similar results were seen.

This synthesis result could potentially be achieved using a more conventional  $\ell_2$ -norm regularisation, as also shown in [16, 17]. However, since the  $\ell_2$ -norm penalisation cannot introduce sparsity in the source vector, no investigation for the optimum source geometry could be done and, therefore, the non-zero sources found in this paper would have to be chosen beforehand.

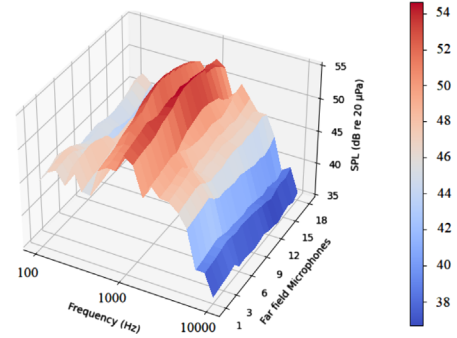


**Figure 19.** SPL at the various frequency bins and across the far field microphone array for the case of two fixed equivalent sources.

## 6 Conclusions

In this paper, the frequency-averaged  $\ell_1$ -norm regularisation approach to the inverse method for predicting the tyre noise response in a pass-by noise context was further extended to a power-based formulation, and was investigated for tyre noise measured spectra for an electric vehicle under accelerating conditions. The measurements took place in a semi-anechoic chamber and involved two different set-ups and run-ups from 5 to 60 km/h at two different accelerations. In the first set-up, only tyre noise from the two front tyres was taken into account, while, in the second set-up, the car was driven in fully operational conditions with noise emitted by the two rear tyres and the gearbox. For both cases, the investigation of the equivalent source number and positioning was done only for the tyre close to the far-field array and the rest of the sources were quantified assuming a fixed small number of equivalent sources. The use of 1, 2, 4 and 8 final non-negligible equivalent sources was investigated for one tyre obtaining correspondingly synthesised responses, which were added energetically to the ones acquired by the remaining sources on the car, and the overall response was compared to the one measured directly.

For the first set-up, where only tyre noise was present, using fixed source positioning gave an acceptable level of synthesis accuracy, with the best accuracy being achieved when using two sources for the left front tyre. The ability of the power-based approach to create larger effective surface patches represented by an average source strength and to avoid the phase errors which have a significant effect on the inversion process, gives good synthesis accuracy by using only one source at each edge of the tyre, which is a substantial improvement compared to the approach where the phase information and source coherence were taken into account, as presented in [20] for steady-speed measured data.

For the second set-up, where tyre and gearbox noise were present, similar conclusions were drawn regarding the optimum number of equivalent sources needed for the power-based approach. The one-source far-field estimate was seen to have a smaller deviation from the directly measured spectra compared to the first set-up, while slight

larger overestimations of the final response were seen when using eight sources. With the aim of minimising the number of sources and targeting the dominant region of 400 Hz to 1.5 kHz, the two-source case was selected as the optimum one, although results of similar accuracy were also seen in the four-source case.

## Acknowledgments

The authors gratefully acknowledge the European Commission for its support of the Marie Skłodowska Curie program through the ETN PBNv2 project (GA 721615). The authors are also grateful to Nikolaos Kournoutos for his precious help with the measurements and to Karl Janssens for fruitful discussions on the experimental campaign.

## Conflict of interest

The authors declare that they have no conflict of interest.

## Data availability statement

The research data associated with this article are available in University of Southampton Institutional Repository, under the reference <http://dx.doi.org/10.5258/SOTON/D1477>.

## References

1. International Organization for Standardization, ISO 362-3:2016: Measurement of noise emitted by accelerating road vehicles – Engineering method – Part 1: M and N categories.
2. J.W. Verheij: Inverse and reciprocity methods for machinery noise source characterization and sound path quantification. Part 1: Sources. *International Journal of Acoustics and Vibration* 2, 1 (1997) 11–20.
3. J.W. Verheij: Inverse and reciprocity methods for machinery noise source characterization and sound path quantification. Part 2: Transmission Paths. *International Journal of Acoustics and Vibration* 2, 3 (1997) 103–112.
4. W. Kropp, F.X. Becot, S. Barrelet: On the sound radiation from tyres. *Acta Acustica United with Acustica* 86, 5 (2000) 769–779.
5. Z.D. Zhang, N. Vlahopoulos, T. Allen, K.Y. Zhang: Development and validation of a computational process for pass-by noise simulation. *International Journal of Vehicle Design* 34, 1 (2004) 12–34.
6. J. Huijssen, R. Hallez, B. Pluymers, W. Desmet: An approach for pass-by noise of automotive vehicles employing numerically evaluated source-receiver transfer functions. *Journal of Sound and Vibration* 332 (2013) 3079–3802.
7. F. Pignol, E. Tijs, D.F. Comesana: Measurement of sound pressure contributions in pass-by-noise tests using particle velocity sensors. *Acta Acustica United with Acustica* 102, 1 (2016) 183–189.
8. A.R. Fleszar, P.J.G. van der Linden, J.R. Johnson, M.J. Grimmer: Combining vehicle and test-bed diagnosis information to guide vehicle development for pass-by noise. *SAE Technical Papers* 2001-01-1565, 2001.
9. K. Genuit, S. Guidati, R. Sottek: Progresses in pass-by simulation techniques. *SAE Technical Papers* 2005-01-2262, 2005.
10. B.K. Kim, S.W. Yoo, H.J. Kim, K. Zwanzig: Prediction of vehicle pass-by noise using indoor measurements. *SAE Technical Papers* 2001-01-1563, 2001.
11. J. Putner, M. Lohrmann, H. Fastl: Contribution analysis of vehicle exterior noise with operational transfer path analysis, in *Proceedings of ICA 2013, Montreal, Canada, 2013*.
12. Z. Chu, H. Wang, C. Chen, H. Yan, R. Kang: Source path contribution analysis for vehicle indoor pass-by noise. *SAE Technical Paper* 2017-01-2247, 2017.
13. K. Janssens, P. Aarnoutse, P. Gajdatsy, L. Britte, F. Deblauwe, H. Van der Auweraer: Time-domain source contribution analysis method for in-room pass-by noise. *SAE Technical Paper* 2011-01-1609, 2011.
14. Y. Ryu, A. Schuhmacher, M. Hirayama, Y. Shirahashi: Contribution analysis of exterior noise with indoor pass-by measurement. *SAE Technical Papers* 2011-26-0062, 2011.
15. A. Schuhmacher, Y. Shirahashi, M. Hirayama, M.Y. Ryu: Indoor pass-by noise contribution analysis using source path contribution concept, in *Proceedings of ISMA2012-USD2012, Leuven, Belgium, 2012*.
16. D. Berckmans, P. Kindt, P. Sas, W. Desmet: Evaluation of substitution monopole models for tire noise sound synthesis. *Mechanical Systems and Signal Processing* 24 (2010) 240–255.
17. A. Schuhmacher, J. Hald, K.B. Rasmussen, P.C. Hansen: Sound source reconstruction using inverse boundary element calculations. *The Journal of the Acoustical Society of America* 113 (2003) 114.
18. W. Kropp, K. Larsson, F. Wullens, P. Homstad, F.X. Becot: The generation of the tyre/road noise, in *Proceedings of ICSV 2003, Stockholm, Sweden, 2003*.
19. F. Wullens, W. Kropp: A three-dimensional contact model for tyre/road interaction in rolling conditions. *Acta Acustica United with Acustica* 904 (2004) 702–711.
20. A. Papaioannou, S. Elliott, J. Cheer: Application of  $l_2$ -norm regularisation techniques in the synthesis of indoor tyre pass-by noise with the inverse method. *Journal of Sound and Vibration* 473 (2020) 115240.
21. D. Malioutov, M. Cetin, A.C. Smith: A sparse signal reconstruction perspective for source localization with sensor arrays. *IEEE Transactions on Signal Processing* 53 (2005) 3010–3022.
22. G.F. Edelmann, C.F. Gaumond: Beamforming using compressive sensing. *The Journal of the Acoustical Society of America* 130 (2011) EL232–EL237.
23. P. Simard, J. Antoni: Acoustic source identification: Experimenting the  $l_1$  minimization approach. *Applied Acoustics* 74 (2013) 974–986.
24. G. Chardon, L. Daudet, A. Peillot, F. Ollivier, N. Bertin, R. Gribonval: Near-field acoustic holography using sparse regularisation and compressive sampling principles. *The Journal of the Acoustical Society of America* 132, 3 (2012) 1521–1534.
25. J. Hald: A comparison of iterative sparse equivalent source methods for near-field acoustic holography. *The Journal of the Acoustical Society of America* 143, 6 (2018) 3758–3769.
26. E. Fernandez-Grande, A. Xenaki, P. Gerstoft: A sparse equivalent source method for near-field acoustic holography. *The Journal of the Acoustical Society of America* 1411 (2017) 532–542.
27. A. Xenaki, E. Fernandez-Grande, P. Gerstoft: Block-sparse beamforming for spatially extended sources in a Bayesian formulation. *The Journal of the Acoustical Society of America* 140 (2016) 1828.

28. E. Fernandez-Grande, L. Daudet, Compressive acoustic holography with block-sparse regularization, *The Journal of the Acoustical Society of America* 143 (2018) 3737.
29. P. Gerstoft, A. Xenaki, C.F. Mecklenbrauker: Multiple and single snapshot compressive beamforming. *The Journal of the Acoustical Society of America* 138 (2015) 2003.
30. E. van den Berg, M.P. Friedlander: Theoretical and empirical results for recovery from multiple measurements. *SIAM Journal of Scientific Computing* 21, 4 (2011) 1201–1229.
31. J. Tropp: Algorithms for simultaneous sparse approximation. Part II: Convex relaxation. *Signal Processing* 86 (2006) 589–602.
32. J. Chen, X. Huo: Theoretical results on sparse representations of multiple measurement vectors. *IEEE Transactions on Signal Processing* 54, 12 (2006) 4634–4643.
33. P.A. Nelson, S.H. Yoon: Estimation of acoustic source strength by inverse methods: Part I: Conditioning of the inverse problem. *Journal of Sound and Vibration* 233, 4 (2000) 643–668.
34. K.R. Holland, P.A. Nelson: The application of inverse methods to spatially-distributed acoustic sources. *Journal of Sound and Vibration* 332 (2013) 5727–5747.
35. K. Shin, J. Hammond: *Fundamentals of Signal Processing for Sound and Vibration Engineers*. Wiley Press, Chichester, UK, 2008.
36. E. van den Berg, M.P. Friedlander: Sparse optimisation with least-squares constraints. *SIAM Journal of Scientific Computing* 21, 4 (2011) 1201–1229.
37. E. van den Berg, M.P. Friedlander: SPGL1: A solver for large-scale sparse reconstruction, 2008. <http://www.cs.ubc.ca/labs/scl/spgl1>.
38. E. van den Berg, M.P. Friedlander: Theoretical and empirical results for recovery from multiple measurements. *IEEE Transactions on Information Theory* 56, 5 (2010) 2516–2527.
39. LMS International: Mid high frequency volume velocity source (Q-MHF): LMS Qsources excitation hardware.

**Cite this article as:** Papaioannou A. Elliott S.J. Cheer J. Cuenca J. & Alkmmim M, et al. 2021. Power-based application of frequency-averaged  $\ell_1$ -norm regularisation technique for the synthesis of accelerating indoor tyre pass-by noise. *Acta Acustica*, 5, 50.